Naphthalimide functionalized metal–organic framework for rapid and nanomolar level detection of hydrazine and anti-hypertensive drug nicardipine†

Sk Sakir Hossain,[a] Dirk Volkmer [b] and Shyam Biswas *[a]

The increasing utilization of hydrazine and its derivatives across diverse sectors highlights the pressing need for efficient detection methods to safeguard human health and the environment. Likewise, nicardipine, a widely used medication for heart diseases, necessitates accurate sensing techniques for clinical research and therapeutic monitoring. Here, we propose a novel approach using a naphthalimide-functionalized Zr-MOF as a fluorometric probe capable of detecting both hydrazine and nicardipine in aqueous medium. Our designed probe exhibited a significant 31-fold increase in fluorescence intensity upon interaction with hydrazine. At the same time, nicardipine induced 86% fluorescence quenching with an exceptionally rapid response time (100 s for hydrazine and 5 s for nicardipine). The designed probe has the ability to detect both analytes at nanomolar concentrations (LOD for hydrazine is 1.11 nM while that for nicardipine is 9.6 nM). Investigation across various wastewater samples and pH conditions further validated its practical utility. The mechanism behind fluorometric sensing of nicardipine was thoroughly investigated using modern instrumentation. Our study presents a versatile and effective approach for detecting hydrazine and nicardipine, addressing crucial needs in both industrial and biomedical contexts.

Introduction

Hydrazine and its derivatives have received more attention day by day in various fields of agriculture, fuels, aerospace, catalysis, *etc*.[1] It serves as a versatile building block in chemical synthesis, particularly in the production of pharmaceuticals, agrochemicals, and specialty chemicals. It is used as a precursor in the synthesis of various compounds, including pharmaceutical intermediates and pesticides. It is employed in boiler water treatment to remove dissolved oxygen and prevent corrosion in steam-generating systems.[2] It is also widely used as a rocket fuel due to its high energy content and ability to undergo exothermic decomposition.[3] Apart from rocket propulsion, hydrazine is also used in other aerospace applications, such as altitude control systems in satellites and spacecraft.[4] Despite its huge number of applications, hydrazine is a hazardous material and is considered as carcinogenic for humans. Its accumulation in the environment occurs through the discharge of industrial waste. Detecting hydrazine in water is imperative due to its potential hazards to human health and the environment. Hydrazine, even in low concentrations, poses significant risks, including skin and eye irritation, respiratory issues, and organ damage upon exposure through contaminated water sources.[5] In animals, it was observed that hydrazine could affect their spinal cord, liver, DNA, brain, and kidneys and might cause injury to the lungs.[6] Moreover, hydrazine pollution can disrupt aquatic ecosystems, harming aquatic life and jeopardizing biodiversity. Effective monitoring of hydrazine levels in water is essential for safeguarding public health, preserving environmental integrity, and ensuring regulatory compliance. Continuous monitoring enables early detection of pollution incidents, facilitating prompt response actions to mitigate contamination spread and minimize adverse impacts. The threshold concentration of hydrazine in drinking water has been set at 10 ppb.[7] Therefore, the detection of hydrazine below the safe limit is highly required.

In the modern days, especially after COVID-19, different kinds of drugs have been extensively used all over the world to make humans healthy.[8] Nicardipine (1,4-dihydro-2,6-dimethyl-4-[3-nitrophenyl]-3,5-pyridinecarboxylic acid, methyl-2-[methyl (phenylmethyl)amino]ethyl ester) is one such medication. It

[a]*Department of Chemistry, Indian Institute of Technology Guwahati, Guwahati, 781039 Assam, India. E-mail: sbiswas@iitg.ac.in*
[b]*University of Augsburg, Institute of Physics, Chair of Solid State and Materials Chemistry, Universitaetsstrasse 1, 86159 Augsburg, Germany*

†Electronic supplementary information (ESI) available: NMR spectra, ATR-IR spectra, PXRD profiles, TGA plots, EDX spectra, N_2 sorption isotherms, FESEM image, fluorometric sensing results, UV-Vis spectra and comparison tables. See DOI: https://doi.org/10.1039/d4dt00818a

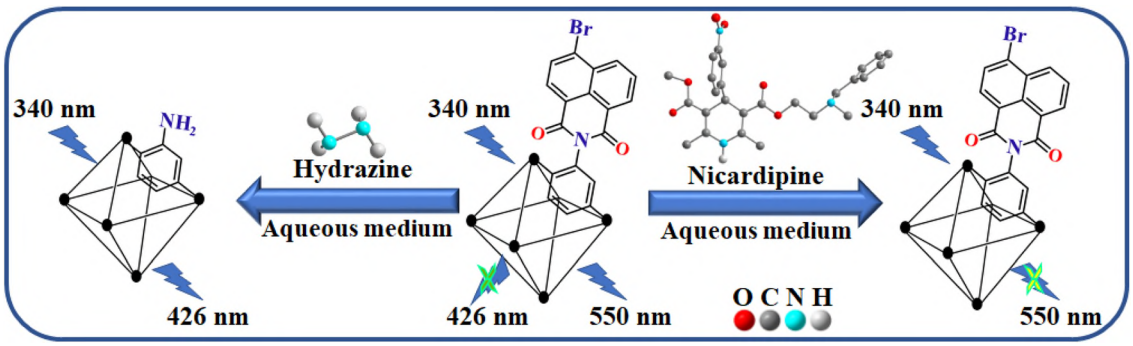

Scheme 1 Fluorescence turn-on mode sensing of NH_2NH_2 and turn-off mode sensing of nicardipine using probe **1′** in aqueous medium.

belongs to a class of 1,4-dihydropyridine calcium channel antagonists that play crucial roles in the treatment of heart diseases like angina pectoris and arterial hypertension.[9] Nicardipine sensing is valuable for clinical research studies investigating its pharmacokinetics, pharmacodynamics, and therapeutic efficacy in different patient populations.[10] Accurate measurement of nicardipine concentrations allows researchers to assess its bioavailability, distribution, and elimination profiles. Monitoring nicardipine levels in patients undergoing treatment is essential to ensure proper dosing and effectiveness of the medication. Too little nicardipine may lead to inadequate control of hypertension or angina, while too much can cause adverse effects such as hypotension or dizziness.[11] Detecting nicardipine levels can help prevent potential drug interactions or adverse reactions when taken concomitantly with other medications. Certain drugs or substances may affect nicardipine metabolism or clearance, leading to altered drug levels in the body. Pharmaceuticals like nicardipine can enter wastewater through excretion by humans, improper disposal, or incomplete removal during wastewater treatment processes.[12] Nicardipine and other pharmaceuticals in wastewater can persist in the environment and pose risks to water quality. Monitoring nicardipine levels provides insights into the presence and persistence of these contaminants, aiding in the assessment of water quality and potential health risks associated with exposure. Because many of these drugs are highly potent and effective at low doses, highly sensitive as well as high selective sensor is required for therapeutic monitoring and pharmacokinetic studies.

Different types of analytical methods were introduced for the detection of above mentioned analytes, like chromatographic, electrochemical, spectroscopic and fluorescence methods *etc.*[13–16] Among the above-mentioned methods, the fluorometric method has various advantages due to its easy handling and simple evaluation process.[15] Many classes of fluorometric sensors materials have been used for the sensing of hazardous materials and drugs including quantum dots, graphene oxide-based materials, carbon nanotubes, metallogel, organic probes, and metal–organic frameworks (MOFs).[17–21] Among them, MOFs nowadays have become a promising class of sensors for detecting several important analytes due to their porous nature with very high surface area, high stability and tuneable functionality.[22,23]

Hydrazine exhibits a moderate degree of nucleophilicity. This fact simulated us designing an MOF-based probe with a moderately electrophilic centre within the framework.[24] We observed that nicardipine has λ_{max} at 350 nm. Therefore, if a fluorometric probe is excited close to λ_{max} of nicardipine, this excitation can facilitate the detection of nicardipine *via* a non-radiative energy transfer pathway. Stimulated by the above ideas, we applied the activated form of a novel naphthalimide-functionalized Zr(IV)-MOF (**1′**) for detection of industrial hazardous hydrazine and a widely used anti-hypertensive drug nicardipine (Scheme 1) in water medium. Our designed probe showed a 31-fold increment of fluorescence intensity upon the addition of hydrazine to the MOF while 86% fluorescence quenching phenomenon occurred in presence of nicardipine. The probe showcased an exceptionally rapid response time for detecting both target analytes and demonstrated the capability to identify them at nanomolar concentration. The probe's capability to sense the targeted analytes was investigated across various wastewater samples and under different pH conditions. For real field applications, nicardipine sensing was executed in real biological samples (human serum and urine). The mechanistic pathway of sensing was explored in details with help of modern instrumental techniques. The practical suitability, specificity, and remarkably low detection limit distinguish our designed probe as particularly effective for detecting NH_2NH_2 and nicardipine.

Experimental section

Synthesis of $[Zr_6O_4(OH)_4(C_{20}H_8BrNO_6)_3(C_2O_2F_3)_6]\cdot 7H_2O\cdot 2.5DMF$ (1)

The synthesis procedure for the linker is detailed in the ESI.† The solvothermal method was adopted for the synthesis of MOF. Typically, a 15 mL Pyrex tube was filled with 46 mg (0.14 mmol) of $ZrOCl_2\cdot 8H_2O$, 56 mg of the synthesized linker (0.14 mmol) and 320 μL (4.2 mmol) of trifluoroacetic acid, and 3 mL of DMF. The sealed tube is sonicated for 15 min and placed in a preheated block heater at 150 °C for 24 h. After

that, a dark yellowish precipitate was obtained by filtration. The unreacted starting materials were removed by washing it with DMF and, finally, with acetone. The final product was overnight drying in a hot air oven at 80 °C. Yield of **1** based on Zr salt: 0.03 g (0.01 mmol, 55%). Anal. Calcd for $C_{79.5}H_{59.5}5Br_3F_{18}N_{5.5}O_{47.5}Zr_6$ (2944.33 g mol^{-1}): C, 31.82; H, 1.92; N, 2.38. Found: C, 31.51; H, 1.84; N, 2.31%. ATR-IR (cm^{-1}): 3411 (br), 1698 (w), 1643 (w), 1581 (s), 1505 (vs), 1244 (m), 1182 (w), 1010 (w), 770 (m), 646 (vs).

Activation of freshly synthesized MOF (1)

The as-synthesized MOF (**1**) was activated in the following way. At first, 50 mg of **1** was suspended in a 20 mL of MeOH and kept it for 24 h under stirring conditions for solvent exchange. After one day, the mixture was filtered and subsequently put in a hot-air oven at 100 °C and finally vacuum-dried at 100 °C for 24 h to get the activated MOF (**1′**).

Results and discussion

Structural interpretation

The reaction between Zr(IV) salt and terephthalic acid leads to mainly two types of MOFs such as MIL-140A and UiO-66.[25,26] Among them, the later one has been widely investigated for various applications for its high chemical and thermal stability. In this MOF, the Zr_6-oxo cluster acts as secondary building unit (SBU) of the framework. The SBU has the formula $[Zr_6O_4(OH)_4]$. They are bridged by terephthalate ligands. In this cluster, each Zr(IV) ion has a coordination number of 8, resulting in a square antiprismatic geometry. These eight coordination sites are fulfilled by eight oxygen atoms. These oxygen atoms comprise of four carboxylate oxygen atoms from four distinct terephthalate linker, two from μ_3-O and the other two from μ_3-OH units. Each SBU is coordinated with 12 linkers. Therefore, it is a 12-conneted framework. But, it has been reported that ideally 12-connected framework is not possible for the terephthalate linker with bulky functionality due to steric repulsion. For example, Rapti *et al.* reported an 8-connected Zr(IV)–organic framework containing bulky functional group grafted with terephthalate linkers.[27] This framework has four linkers missing from each Zr_6 oxocluster. Similarly, several 6-conneted Zr(IV) MOFs with terephthalate linkers having long chain alkyl groups were reported by Pournara *et al.* where six linkers were missing from each Zr_6 oxocluster.[28] We synthesized the MOF with Zr(IV) salt and terephthalic acid linker having bulky naphthalimide functionality (**1**). Therefore, we expected that the obtained MOF would have similar type linker defects in the framework. We tried to find the linker defects from thermogravimetric analysis (TGA) by following the reported procedure and found that the obtained MOF has a 6-connected framework (Fig. 2a and b).[29] The vacant linker defect sites are occupied by six trifluoroacetate (modulator) anions for each Zr_6 cluster, which was proved by EDX (Fig. S4†) and ^{19}F NMR (Fig. S11†) analysis. Based on these experimental results, we modelled the solvent-free structure of compound **1** by molecular mechanics, employing the universal force field (UFF) as implemented in the Forcite software module of Biovia Materials Studio.[30] The reported MOF structure served us as starting point for homology modelling of the unknown structure of **1**.[28] The obtained crystallographic information (CIF) file is provided in ESI.† The experimentally obtained PXRD pattern was similar to the simulated PXRD pattern of **1** (Fig. 1a). The high structural resemblance between **1** and the simulated structure was further proved by the Pawley refinement (Fig. 1b) of the PXRD data of **1′**. The lower values of R_p = 1.7% and R_{wp} = 0.9% suggested the closeness between the experimental and simulated PXRD profiles of **1′**. There are two different types of cages can be found in the framework structure (Fig. 2c and d): larger sized octahedral and smaller sized tetrahedral cavities.

Field emission scanning electron microscopy (FE-SEM) is an advanced technique employed to capture microstructural images of materials. The framework morphology of **1** was examined by FE-SEM image. In the FE-SEM image of **1′**, a homogeneous distribution of octahedral particles was

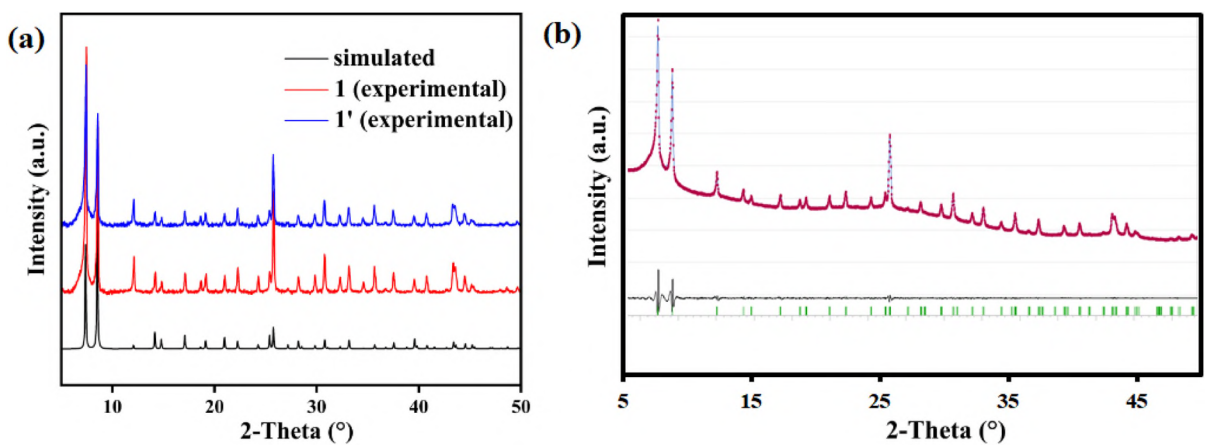

Fig. 1 (a) PXRD profiles of **1** and **1′** compared with simulated one. (b) Pawley refinement of PXRD profile of **1′** (R_{wp} and R_p are 1.7% and 0.9%, respectively).

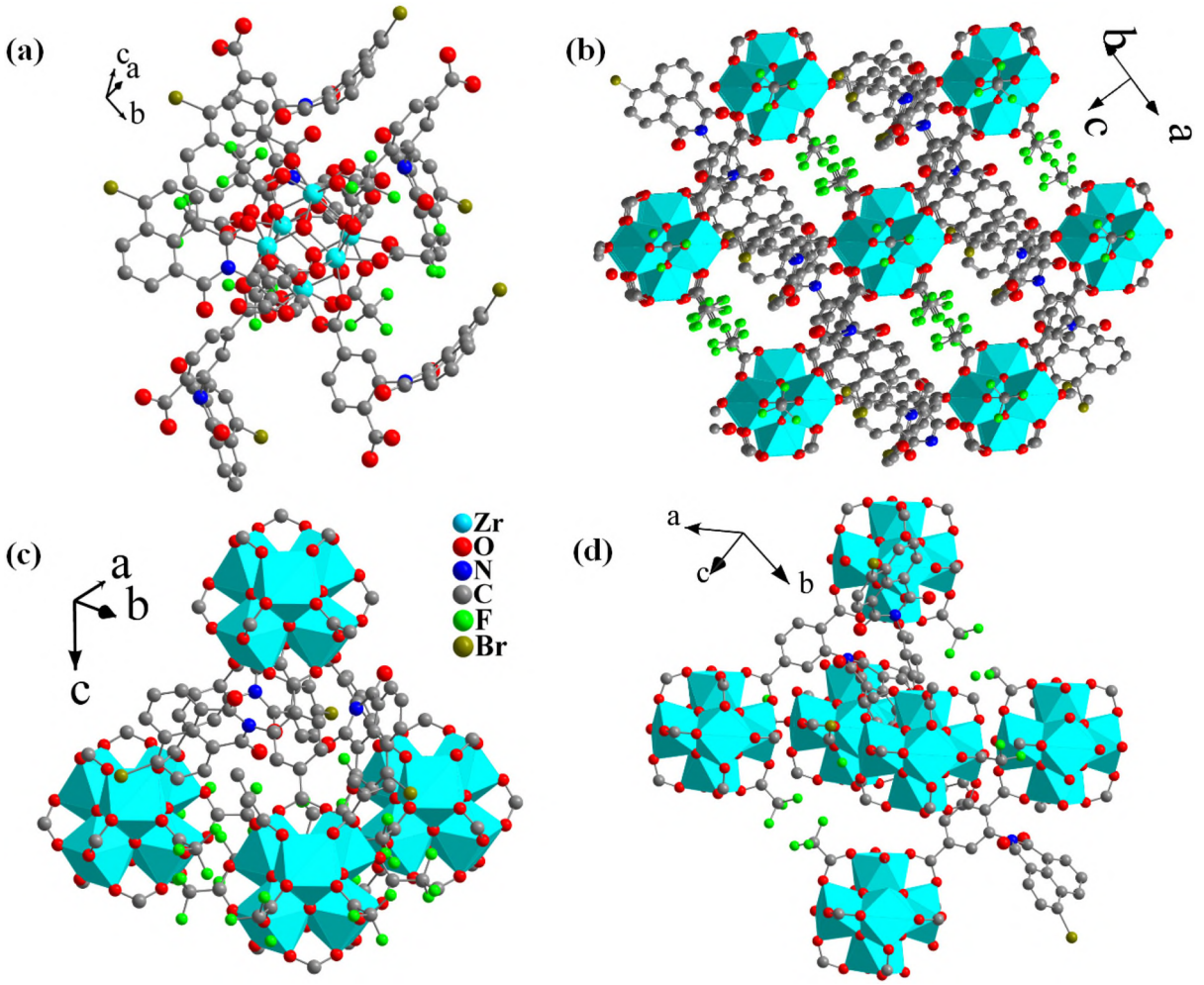

Fig. 2 (a) View of the SBU present in the framework of **1**. (b) View of the complete structural framework of **1**. (c and d) Tetrahedral and octahedral voids present in the framework of **1**.

observed (Fig. 3a). The presence of the desired elements in **1** was confirmed through energy dispersive X-ray (EDX) analysis, as depicted in Fig. 3c. The uniform distribution of these elements was further demonstrated by EDX elemental mapping (Fig. 3d).

Functional group analysis

Previous studies have indicated that the stretching mode vibrational frequency of 'C═O' bond in carboxylic acids shifts to a lower wavenumber when they bind to a metal centre, owing to the interaction between the carbonyl group and the metal centre. In our experiment, we conducted ATR-IR analysis to verify this phenomenon.[31] We observed that the abovementioned peak appeared at 1574 cm^{-1} for both **1** and **1′**, but for the linker, it was observed at 1588 cm^{-1} (Fig. S3†). This shift in the C═O stretching frequency suggests the binding of the carboxylate group with the Zr_6 nodes. Furthermore, the MOF was subjected to digestion using HF, followed by collection of ^1H NMR data. The resemblance observed between the ^1H NMR data obtained for the H_2L ligand and the digested sample of **1** confirmed the preservation of the desired functionality in **1′** throughout the MOF synthesis process (Fig. S4†).

Chemical tolerance of 1′

The stability of the sensor in various chemical environments, particularly in the sensing medium, was assessed thoroughly investigated. First, we suspended **1′** in different organic solvents, water and solutions of varying pH. After that the suspensions were kept under stirring condition at room temperature for 24 h. We collected PXRD patterns of the recovered samples after stirring in the mentioned conditions. The results, as depicted in Fig. 3b, unequivocally indicated the remarkable stability of the sensor under these chemical environments.

Thermal tolerance of 1′

To evaluate the thermal stability, TG analysis was performed under a O_2 atmosphere with a heating rate of 4 °C min^{-1} for both **1** and **1′**. The TGA curve of **1** revealed three distinct weight loss stages (Fig. S5†). Initially, within the temperature range of 30–130 °C, a weight loss of 6.2% was observed. This

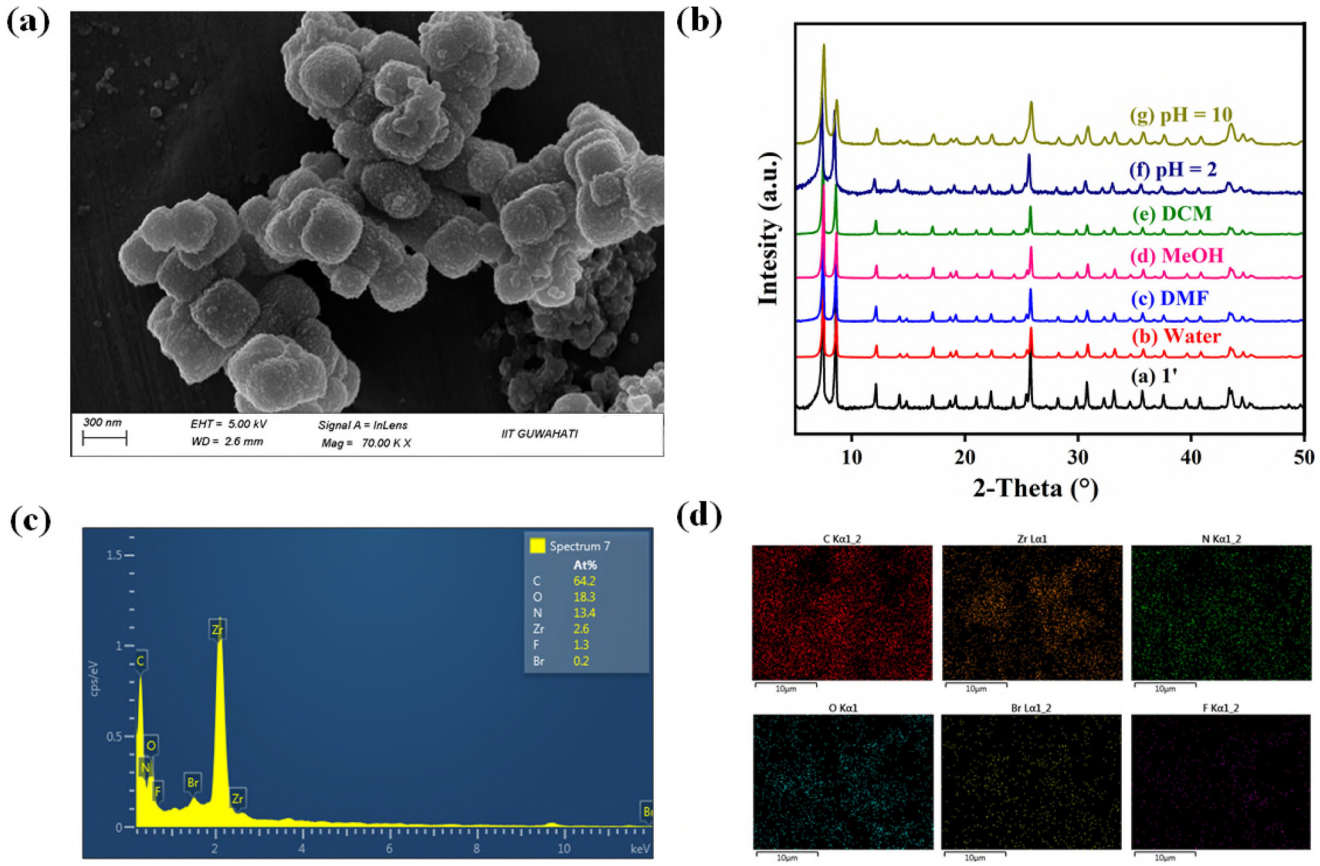

Fig. 3 (a) FESEM image of **1′**. (b) PXRD patterns of **1′** and the obtained samples after stirring in different solvents. (c) EDX spectrum of **1′**. (d) EDX elemental mapping of expected elements present in **1′**.

weight loss was due to elimination of 7.0 water molecules for single unit formula of **1** (calculated was 5.7%). Subsequently, between 130 and 300 °C, a weight loss of 8.8% (calculated as 8.0%) occurred due to the release of 2.5 DMF molecules per formula unit. Beyond 350 °C, a sharp weight loss indicated structural breakdown of the framework. In case of **1′**, a weight loss of 2.5% was observed due to removal of 3.2 water molecules, which may be adsorbed during the storage of **1′**. Therefore the synthesized MOF is stable up to 350 °C.

Examination of linker defects

The presence of a bulky functional group in the linker (H_2L) prompts speculation regarding potential defects within the framework structure. TGA is a valuable experiment for assessing such defects in MOFs. To quantify these missing linker defects in **1′**, we employed methodologies from reported literature.[29] It was calculated that the molecular weight of an ideal, dehydroxylated, solvent-free hexanuclear Zr_6 cluster was determined to be 4.4 times higher than that of six ZrO_2 unit. Calculations based on TGA (given in the ESI†) showed that the experimental plateau ($W_{Exp.\ Plat.}$) was located at 255%, in contrast to the theoretical plateau ($W_{Ideal.\ Plat.}$) expected at 442% if normalized to 100% (Fig. S6†). This discrepancy suggests a lower density in the synthesized framework compared to that predicted by the idealized equation. We concluded from these calculations that there are approximately three linkers defects per formula unit. This result suggests that six linkers are missing from each Zr_6 oxocluster and the vacant linker defect sites are occupied by trifluoroacetate anions. The presence of trifluoroacetate anions was confirmed though EDX (Fig. 3c) and ^{19}F NMR (Fig. S7†) analysis of the activated MOF.

Surface area analysis of 1′

The porous nature of the MOF was investigated through surface area analysis. To explore this characteristic, we conducted N_2 sorption analysis of **1′** at a temperature of −196 °C to assess its surface area (Fig. S8†). The density functional theory pore-size distribution plot (Fig. S8†) confirmed the microporous nature of the framework. The surface area and average pore radius of **1′** were found to be 276 $m^2\ g^{-1}$ and 7.7 Å, respectively. The obtained surface area is notably lower than that of the un-functionalized MOF. Interestingly, prior studies reported that functionalized MOF has lower surface area than that of unfunctionalized one.[32] This phenomenon arises due to the blocking of pores of the MOF by the functional groups. Our findings align with these previous observations, underscoring the impact of functionalization on the porous nature of the MOF.

Fluorometric detection of NH_2NH_2 in water

Water was selected as the sensing medium for our study, and accordingly, the MOF suspension was prepared in water following the procedures outlined in the ESI.† All fluorescence experiments were conducted using this suspension. To perform the fluorometric titration experiment for hydrazine detection, we mixed 3 mL of water with 300 μL of the prepared MOF suspension, and then added 10 mM of the analyte solution into the suspension. The excitation wavelength for all the sensing experiments was set at 340 nm, and the emission spectra were recorded in the 360–610 nm range. The excitation and emission spectra of the MOF suspension in water have been supplemented in Fig. S9.†

A volume-dependent fluorometric titration experiment was performed to evaluate the optimal volume of the 10 mM NH_2NH_2 solution that would result in the maximum fluorescence turn-on phenomenon. The turn-on efficiency was calculated with respect to the emission intensity for 426 nm. This experiment involved gradually adding 25 μL increments of the 10 mM NH_2NH_2 solution to the MOF suspension (3300 μL). As shown in Fig. 4a, the fluorescence emission intensity of the probe increased gradually with the addition of NH_2NH_2 solution. The However, after adding 150 μL of the NH_2NH_2 solution, no further increment in fluorescence intensity occurred. The increment of fluorescence intensity with addition of hydrazine was calculated using the formula I_0/I (where I_0 is the fluorescence intensity of the probe before addition of analyte whereas I_0 refers to intensity post-addition of analyte). After the addition of 150 μL NH_2NH_2 solution, a 31-fold enhancement in fluorescence intensity was observed.

The response time of **1′** towards hydrazine was also examined by time-dependent fluorescence study. In this experiment, 150 μL of 10 mM NH_2NH_2 solution was added to the MOF suspension, and the emission intensity of **1′** was recorded at 5 s intervals. The results revealed a significant 25-fold fluorescence turn-on within 50 s of introducing 150 μL of 10 mM NH_2NH_2 solution. No further increment was observed beyond 100 s, as depicted in Fig. 4b.

To further validate this observation, we performed a fluorescence kinetic experiment, where we recorded the emission intensity of **1′** at 426 nm with time (up to 50 s) upon excitation at 340 nm. After that we added 150 μL of 10 mM NH_2NH_2 solution and the emission intensity was acquired up to 300 s. As shown in Fig. S10,† 25-fold turn-on of fluorescence occurred within the initial 50 s, confirming the ultrafast detection time of our probe for targeted analyte. Based on these results, we can conclude that our synthesized probe **1′** exhibits an exceptionally rapid response time for detecting hydrazine in compared to other reported fluorometric probes (Table S3†).

Selectivity test is an important experiment for any type of sensor. Therefore, the selectivity of **1′** towards NH_2NH_2 was also examined in presence of various competitive analytes like urea, thiourea, NaI, $NaHSO_3$, NaSCN, $NaHCO_3$, $Na_2S_2O_3$, $NaNO_2$, $NaNO_3$, *etc.* (Fig. S11–S26†). For this experiment, 150 μL solution of every interfering analyte (10 mM) was introduced to the MOF suspension, followed by the addition of 150 μL hydrazine solution. As shown in Fig. 5, every analyte had a turn-on efficiency less than 3-fold, except NH_2NH_2 which showed 31-fold turn-on. Moreover, the fluorescence turn-on of the probe was not significantly affected by of other interfering analytes (Fig. S27†).

The limit of detection (LOD) is a crucial characteristic for a sensor to examine its sensitivity. To evaluate it for hydrazine sensing, we conducted sensing experiments across the lowest

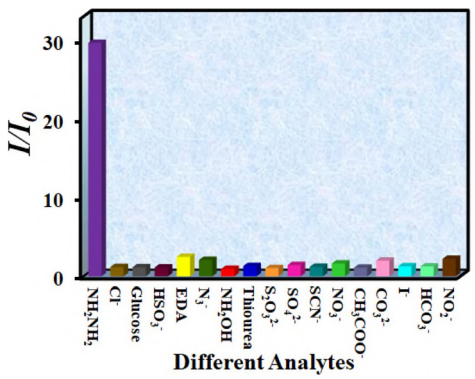

Fig. 5 Comparative bar plots of **1′** towards NH_2NH_2 sensing with its competitive analytes.

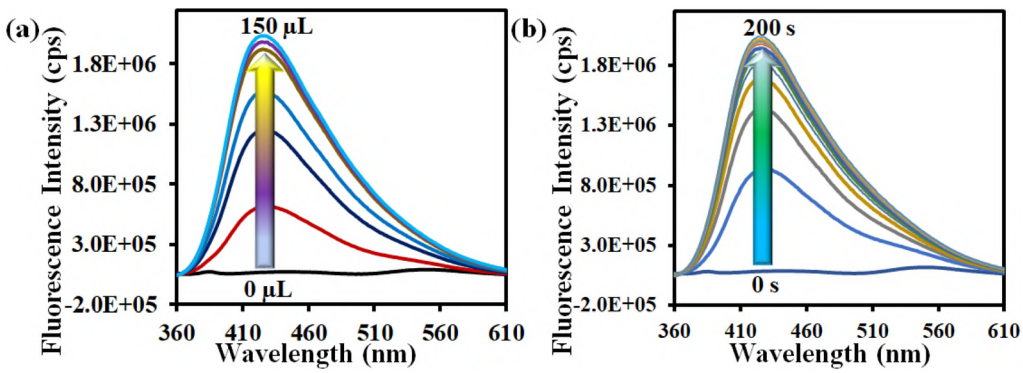

Fig. 4 (a) Volume dependent fluorometric titration for hydrazine sensing. (b) Time dependent fluorescence study for hydrazine sensing.

possible concentration ranges. To determine the LOD, we employed the formula $3\sigma/k$, where σ represents the standard deviation of 10 blank fluorescence readings of the MOF suspension, and k denotes the slope of the linearly fitted plot of emission intensity of **1′** against the concentration of analytes, as shown in Fig. S28.† After performing the calculations, we found that the LOD value for hydrazine was determined to be impressively low as 1.11 nM, which is the lowest among all the fluorescence-based sensors reported to date (Table S3†).

This result demonstrates that our sensor exhibits an exceptional sensitivity, allowing it to detect very low concentrations of the analyte. The ability to achieve such a low LOD makes our sensor highly promising for various practical applications and sets it apart from other fluorescence-based sensors in the field.

Detection of NH_2NH_2 in different pH media and wastewater specimens

We systematically investigated the detection of hydrazine in various pH media. Initially, we prepared the MOF suspension in different pH conditions, ranging from 2 to 10 (Fig. S29†). Subsequently, we added 150 μL of 10 mM hydrazine to each suspension and recorded the fluorescence emission intensity. Our observations revealed that the probe exhibited excellent detection capabilities for hydrazine within the pH range of 2 to 10. In this moderate acidic to slightly basic pH range, the response of probe towards hydrazine was remarkable, leading to significant fluorescence turn-on. However, at extremely acidic conditions (pH = 2), the results were less pronounced, with only a 1.2-fold increase in fluorescence intensity. This can be attributed to the protonation of hydrazine at such low pH levels, causing a loss of its nucleophilicity and inhibiting its ability to efficiently interact with the electrophilic centre. Therefore, based on these observations, it is evident that the detection of hydrazine by our probe is excellent in the pH range of 4 to 10, providing reliable and sensitive results within this favourable pH window.

Hydrazine detection in various real water specimens (Milli-Q, tap, river and lake water) was also explored. At first, **1′** was suspended in the abovementioned water samples. Then, the sensing experiments were performed with hydrazine solutions having concentrations of 1 mM, 5 mM and 10 mM. The emission intensity of **1′** in different water specimens was recorded before and after the addition of hydrazine. The outcomes in terms of fluorescence turn-on are displayed in Fig. S30.† The results confirmed that our probe is highly efficient in detecting hydrazine even in complicated aqueous systems.

Fluorometric nicardipine sensing in water

The detection of nicardipine followed a similar protocol with some modifications. In this instance, emission spectra were acquired within the 490–630 nm range, utilizing the same excitation wavelength employed for hydrazine sensing. Similarly, a volume-dependent sensing experiment was conducted to detect nicardipine in an aqueous medium. This involved incremental additions (50 μL for each step) of a 5 mM nicardipine solution. Gradual increase in concentration of nicardipine decreases the emission intensity at 550 nm. The lowest emission intensity of **1′** was observed after the addition of 300 μL of the 5 mM nicardipine solution, as depicted in Fig. 6a. The quenching efficiency was calculated using the reported formula $(1 - I/I_0) \times 100$. It was determined that the probe's fluorescence intensity decreased by 86% after the introduction of 300 μL of the 5 mM nicardipine solution. The response time of **1′** towards nicardipine sensing was investigated in a similar way to that of hydrazine. Remarkably, it was noted that the fluorescence intensity experienced an 86% reduction within 5 s upon the introduction of 300 μL of a 5 mM nicardipine solution (Fig. 6b). This was further validated by kinetic experiments (Fig. S31†). Consequently, it can be inferred that our probe exhibits an exceptionally rapid detection time for nicardipine sensing.

To assess the selectivity towards nicardipine, a solution of 300 μL of individual competitive analytes (each at a concentration of 5 mM) was added to the MOF suspension. After that, 300 μL of a 5 mM nicardipine solution was introduced. The interfering analytes tested against nicardipine included glucose, urea, K^+, Na^+, Mg^{2+}, Mg^{2+}, Cu^{2+}, Co^{2+}, Zn^{2+}, Cd^{2+}, NO_3^-, CH_3COO^-, SO_2^- *etc.* (Figs. S32–S43†). As illustrated in Fig. 7, no analyte exhibited more than 20% quenching efficiency, with the exception of nicardipine, which displayed a remarkable quenching efficiency of 86%. Furthermore, the presence of various analytes did not impede the nicardipine sensing ability of **1′** (Fig. S44†).

The Stern–Volmer constant (K_{SV}) directly correlates with the quenching efficiency of a quencher. A higher K_{SV} value indicates greater quenching efficiency of a quencher, and *vice versa*. We obtained a plot where I_0/I as a function of analyte concentration of nicardipine to determine the K_{SV} values for its sensing (refer to Fig. S45†). The calculated K_{SV} value was found to be 1.50×10^6 M^{-1} for nicardipine. The high K_{SV} value suggests strong interactions between the probe and nicardipine. Additionally, the 3D Stern–Volmer plots of the targeted analytes (illustrated in Fig. S46†) indicate the high selectivity of our sensor towards nicardipine. To assess the ability of our sensor to detect very low concentrations of nicardipine, we conducted fluorescence experiments across concentration ranges as minimized as possible. The LOD of **1′** for nicardipine sensing was evaluated in the previously mentioned way for hydrazine (Fig. S47†). The calculated LOD value was found to be 9.6 nM for nicardipine. This is the first MOF-based fluorometric nicardipine sensor.

Nicardipine detection in different real water samples and wide pH range

Nicardipine sensing was explored across various real water samples. These experiments were performed in a similar way to that of hydrazine sensing. The results demonstrated that the quenching efficiency of nicardipine remained consistent even in complex aqueous environments (Fig. S48†). Furthermore, we investigated the sensing capability of **1′** across a wide range of pH levels. Our designed probe demon-

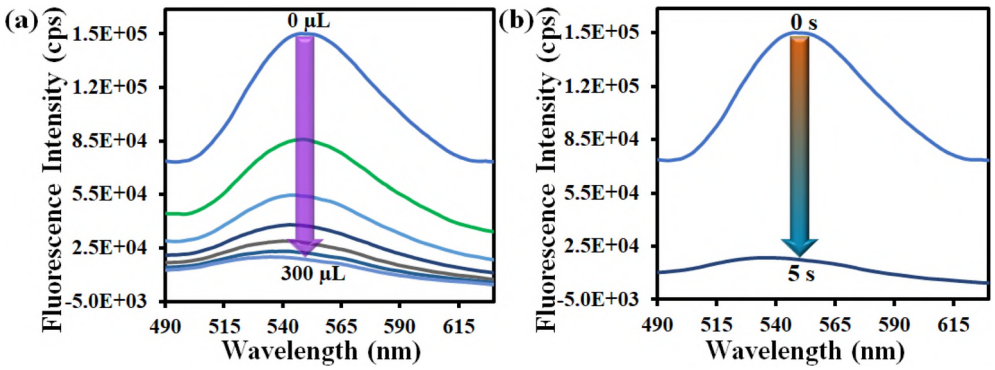

Fig. 6 (a) Change of fluorescence intensity of **1′** with incremental addition of nicardipine solution in water. (b) Time dependent fluorescence study for nicardipine sensing.

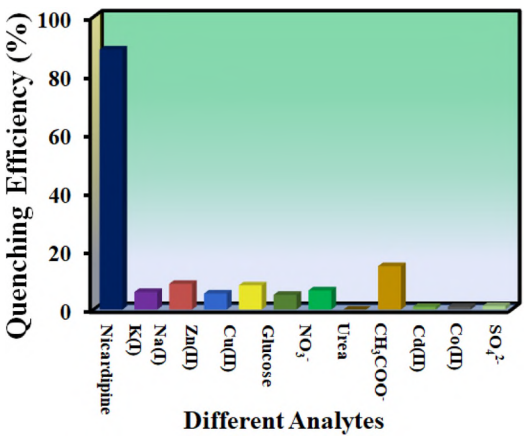

Fig. 7 Comparative bar plots of **1′** towards nicardipine sensing with its competitive analytes.

strated the ability to detect nicardipine over a broad pH range (from 2 to 10) without experiencing a significant loss in its quenching efficiency, as illustrated in Fig. S49.†

Detection of nicardipine in urine and blood serum

Nicardipine detection was extended to more complex media such as human urine and human blood serum. Elaborate instructions for the preparation of urine and blood serum samples can be found in the ESI.† Nicardipine was added to various serum and urine samples, and these solutions were then added to **1′** suspension and its fluorescence intensity was measured. Each experiment was conducted thrice to assess the relative standard deviation (RSD) of the measurements. The experimental outcomes are summarized in Tables S1 and S2.† Remarkably, in these mentioned media, the recovery percentages ranged between 98.0% and 106.0% with relatively low RSD (0.8% to 1.9%). These results indicate that our probe is efficient in detecting nicardipine in complex media.

Reusability of sensor

The recyclability of **1′** for both the analytes was thoroughly investigated. After every cycle of sensing, the MOF was collected through centrifugation and washed with large excess of water to remove the analytes. Following centrifugation and rinsing with excess water, the acquired MOF was employed for the subsequent cycle. The results revealed that **1′** has lost its efficiency for hydrazine sensing after one cycle and continued to the 3rd cycle (Fig. S50†). In a similar way, we investigated the reusability of the probe for nicardipine sensing. The probe showed reusability up to the 4th cycle without significant loss of its efficiency (Fig. S54†). We recorded the PXRD data of the recovered MOF after sensing of each analyte to check its stability after sensing. The PXRD patterns remained the same even after sensing (Fig. S51†). We also collected the FESEM images of **1′** after sensing to check the morphology after sensing (Fig. S52 and S53†). There was a significant change in morphology of **1′** after the sensing of hydrazine but it remained almost same after nicardipine sensing (Fig. S54†). All these observations indicated reaction-based phenomenon for hydrazine sensing and non-reaction-based nicardipine sensing.

Mechanism of fluorometric hydrazine sensing

The probable mechanism for the selective detection of hydrazine was thoroughly investigated with the help various analytical techniques. After going through several literature, we concluded that various processes might cause the enhancement of fluorescence intensity of the probe in presence of a specific analyte, like PET, breaking of MOF structure, and chemical reaction, *etc.*[33] It is previously mentioned that the MOF was stable (from PXRD patterns) after the first cycle of sensing (Fig. S51†) and lost its reusability. This result omits the possibility of the first two mentioned possibilities (*i.e.* PET and destruction of framework) of sensing. The non-reusability of the probe toward hydrazine sensing indicated that the hydrazine reacts with the probe in irreversible way and generates a new species which is highly fluorescent. The reaction between **1′** and NH_2NH_2 was examined in details. The EDX analysis of the recovered MOF after hydrazine sensing indicated the absence of 'Br' element in the resulting MOF (Fig. S55†). The exceptional selectivity of our sensor for hydrazine detection is primarily attributed to the presence of the naphthalimide group within the probe's structure. Upon interaction with

hydrazine, the naphthalimide group undergoes cleavage, leading to the formation of a primary amine group. This breaking resulted in a highly fluorescent 2-aminoterephthalate moiety (Scheme 2). The transformation occurred mainly through a well-established reaction pathway known as the Gabriel reaction. This reaction has been widely utilized to design small organic molecules for hydrazine sensing.[34] This unique behaviour of the probe, arising from the specific chemical reactivity of the naphthalimide group with hydrazine, enables highly selective and sensitive detection of the target analyte.

The proposed mechanism was proved in two different ways. Firstly, we treated the MOF with hydrazine and then washed several times with DMF and water. The recovered MOF was digested with 40% HF in DMSO-d_6 and then we recorded the ^{1}H NMR spectrum of it. The result supported the complete disappearance of naphthalimide peak in the ^{1}H NMR spectrum (Fig. S56†). Secondly, we treated the pure linker with hydrazine and then washed several times with water. The obtained product was collected and characterized with ^{1}H NMR measurement. In the ^{1}H NMR spectrum, there was no peak of BDC (1,4-benzene dicarboxylic acid) protons (Fig. S57†). Additionally, the 'Br' atom was substituted with hydrazine from naphthalimide. All these observations support the proposed mechanism of hydrazine sensing using the probe **1′**.

Mechanism of nicardipine sensing

In our study, we conducted a thorough investigation into the precise mechanisms underlying the selective recognition of nicardipine by our probe **1′**. Given that our probe exhibited a turn-off response to nicardipine, our attention was primarily directed toward understanding turn-off based quenching mechanisms. To unravel these mechanisms, we delved into existing literature, exploring various phenomena that could potentially contribute to fluorescence turn-off, such as structural alterations within the MOF, complexation phenomena, chemical reactions occurring upon interaction with nicardipine, the inner filter effect (IFE), photo-induced electron transfer (PET), and fluorescence resonance energy transfer (FRET).[32,35]

To validate the stability of probe **1′** after nicardipine sensing, we employed PXRD analysis to scrutinize any potential structural changes (Fig. S51†). Remarkably, the results demonstrated that the probe maintained its structural integrity post-sensing, effectively ruling out the possibility of structural disruption during the sensing process. Additionally, we assessed the reusability of the sensor for nicardipine detection (Fig. 54†), which further confirmed that the sensing mechanism was not primarily driven by irreversible chemical reactions. The lack of substantial overlap between the emission spectrum of **1′** and the absorption spectrum of nicardipine (depicted in Fig. 8) decisively eliminates the potential for the FRET mechanism. On the contrary, a significant overlap emerged between the excitation spectrum of **1′** and the absorption spectrum of nicardipine, as illustrated in Fig. 8. The possibility of PET was investigated through energy calculation of highest occupied molecular orbital (HOMO) and lowest unoccupied molecular orbital (LUMO) of the free linker and nicardipine. All calculations were performed using the Pople diffuse basis set 6-31G+(d, p) and B3LYP functional. It was observed that the LUMO of the nicardipine has higher energy than that of the linker (Fig. S58†). This result indicates that the PET cannot be the probable reason for fluorometric sensing of nicardipine using **1′**. The IFE could be a plausible explanation for the fluorescence quenching of the MOF in presence of nicardipine. The IFE-based mechanism arises from the absorption of excitation light or emitted fluorescence by components within the sample matrix. When analytes

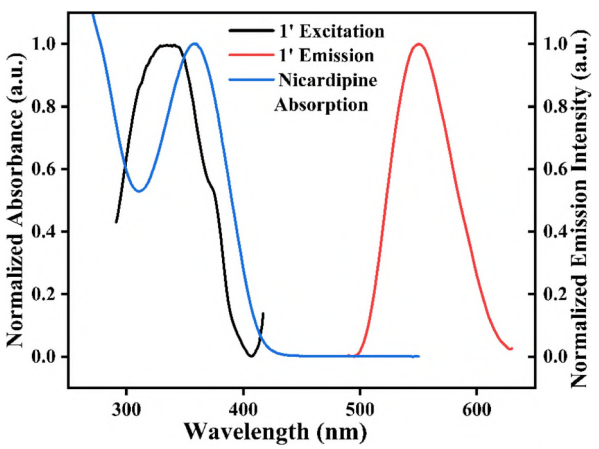

Fig. 8 Spectral overlap among the excitation spectrum of **1′**, emission spectrum of **1′** and UV-Vis absorption of nicardipine.

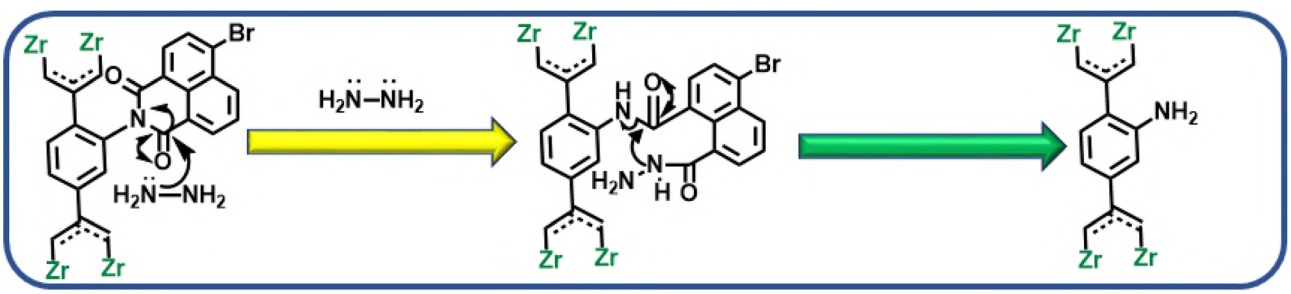

Scheme 2 Probable mechanistic pathway for selective detection of hydrazine by the probe **1′**.

absorb light in the excitation or emission wavelength range of the fluorophore, they can attenuate both the excitation light and the emitted fluorescence, leading to a reduction in fluorescence intensity. IFE can be mitigated by excitation of the probe outside the absorption region of the analytes. Consequently, we excited **1′** at 400 nm and 450 nm and recalculated the quenching efficiency of nicardipine (Fig. S59 and S60†). Surprisingly, a substantial decrease in fluorescence quenching efficiency was observed when the probe was excited at 400 nm or 450 nm instead of 340 nm. This observation confirmed that IFE is the predominant mechanism responsible for the fluorometric selective recognition of nicardipine. In absence of nicardipine, all the incoming photons are experienced by the **1′** during excitation, but in presence of nicardipine, most of the photons are absorbed by nicardipine. As a result, **1′** could not be excited to the full extent. Consequently, turn off of its emission intensity was observed. Once considered an error in fluorescence measurements, IFE has now solidified its position as a non-radiative mechanistic model for energy transfer within spectroscopic methodologies. It has been successfully utilized in the development of various photoluminescence-based sensors.

Conclusion

A novel Zr(IV)-MOF, functionalized with the naphthalimide group, was synthesized *via* a solvothermal method. The resulting functionalized MOF (**1′**) was subjected to thorough characterization. Notably, probe **1′** exhibited highly selective 31-fold fluorescence turn-on behaviour towards hydrazine in aqueous medium, displaying remarkable discrimination against other competitive analytes. Alongside its high selectivity, the probe demonstrated excellent sensitivity towards hydrazine, with a detection limit found to be in the nanomolar level (1.11 nM). The outstanding selectivity of the probe for hydrazine can be attributed to the chemo-selective cleavage of the naphthalimide group, which is grafted with the ligand in the framework, leading to the formation of the corresponding primary amine moiety. This specific chemical reaction serves as the mechanistic pathway for the fluorometric detection of hydrazine by **1′**, and its verification was confirmed through various analytical instrumentation. Along with this, our designed probe could also detect a commonly used drug, nicardipine, in turn-off mode. The fast response time (5 s) and extremely low LOD (9.6 nM) make **1′** an effective sensor for selective and detection of nicardipine. The sensing capability of **1′** was investigated across diverse wastewater samples and under varying pH conditions to detect both analytes effectively. The mechanistic pathway was thoroughly investigated with advanced instrumentation. We have also investigated the nicardipine sensing ability of probe in complex biological media like human serum and urine. This discovery promises to significantly enhance the development of efficient and convenient fluorescent tools for detecting hydrazine and nicardipine, thereby advancing their practical applications.

Ethical statement

All experiments were performed in accordance with the Guidelines for Use of Live Subjects of IIT Guwahati and approved by the ethics committee at IIT Guwahati. Informed consents were obtained from human participants of this study.

Author contributions

SSH performed all the experimental works and prepared the manuscript. DV theoretically optimized the structure of the MOF. Scientific advice was obtained from SB.

Conflicts of interest

There are no conflicts to declare.

Acknowledgements

This project obtained funding from SERB grants CRG/2021/000080 and EEQ/2021/000013. SSH is thankful to PMRF for the financial support.

References

1 A. T. Hoang, A. Pandey, Z. Huang, R. Luque, K. H. Ng, A. M. Papadopoulos, W.-H. Chen, S. Rajamohan, H. Hadiyanto and X. P. Nguyen, *ACS Sustainable Chem. Eng.*, 2022, **10**, 3079–3115.
2 M. M. Rahman, A. Al-Hamzah, A. Al-Sahary, C. M. Fellows and I. M. Al-Farsani, *Water Resour. Ind.*, 2023, **29**, 100212.
3 P. Kumar, *Def. Technol.*, 2018, **14**, 661–673.
4 A. Adami, M. Mortazavi, M. Nosratollahi, M. Taheri and J. Sajadi, *Int. J. Aerosp. Eng.*, 2015, **2015**, 1–8.
5 A. Nair, P. Yadav, A. Behl, R. K. Sharma, S. Kulshrestha, B. S. Butola and N. Sharma, *Chem.-Biol. Interact.*, 2021, **350**, 109654.
6 P. S. Spencer and G. E. Kisby, *Chem. Res. Toxicol.*, 2021, **34**, 1953–1969.
7 S. Paul, R. Nandi, K. Ghoshal, M. Bhattacharyya and D. K. Maiti, *New J. Chem.*, 2019, **43**, 3303–3308.
8 R. K. Guy, R. S. DiPaola, F. Romanelli and R. E. Dutch, *Science*, 2020, **368**, 829–830.
9 T. Godfraind, *J. Cardiovasc. Pharmacol. Ther.*, 2014, **19**, 501–515.
10 M. E. Krecic-Shepard, K. Park, C. Barnas, J. Slimko, D. R. Kerwin and J. B. Schwartz, *Clin. Pharmacol. Ther.*, 2000, **68**, 130–142.
11 W. J. Elliott, *J. Clin. Hypertens.*, 2004, **6**, 587–592.
12 M. Patel, R. Kumar, K. Kishor, T. Mlsna, C. U. Pittman Jr and D. Mohan, *Chem. Rev.*, 2019, **119**, 3510–3673.

13 B. Mutharani, H.-C. Tsai, J.-Y. Lai and S.-M. Chen, *Anal. Chim. Acta*, 2022, **1199**, 339567.
14 K. Zarei, L. Fatemi and K. Kor, *J. Anal. Chem.*, 2015, **70**, 615–620.
15 S. K. Manna, A. Gangopadhyay, K. Maiti, S. Mondal and A. K. Mahapatra, *ChemistrySelect*, 2019, **4**, 7219–7245.
16 Y. Jung, I. G. Ju, Y. H. Choe, Y. Kim, S. Park, Y.-M. Hyun, M. S. Oh and D. Kim, *ACS Sens.*, 2019, **4**, 441–449.
17 B. Liu, J. Zhuang and G. Wei, *Environ. Sci.: Nano*, 2020, **7**, 2195–2213.
18 N. Alam, S. Mondal, S. S. Hossain, S. Sahoo and D. Sarma, *ACS Appl. Eng. Mater.*, 2023, **1**, 1201–1212.
19 M. Singh, A. S. Palakkal, R. S. Pillai and S. Neogi, *J. Mater. Chem. C*, 2021, **9**, 7142–7153.
20 R. Goswami, T. K. Pal and S. Neogi, *Dalton Trans.*, 2021, **50**, 4067–4090.
21 R. Goswami, B. D. Bankar, S. Rajput, N. Seal, R. S. Pillai, A. V. Biradar and S. Neogi, *J. Mater. Chem. A*, 2022, **10**, 4316–4332.
22 P. Kumar, A. Deep and K.-H. Kim, *TrAC, Trends Anal. Chem.*, 2015, **73**, 39–53.
23 S. Ghosh, A. Rana and S. Biswas, *Chem. Mater.*, 2023, **36**, 99–131.
24 V. G. Nenajdenko, N. E. Shevchenko, E. S. Balenkova and I. V. Alabugin, *Chem. Rev.*, 2003, **103**, 229–282.
25 M. Schulz, N. Marquardt, M. Schäfer, D. P. Warwas, S. Zailskas and A. Schaate, *Chem. – Eur. J.*, 2019, **25**, 13598–13608.
26 J. H. Cavka, S. Jakobsen, U. Olsbye, N. Guillou, C. Lamberti, S. Bordiga and K. P. Lillerud, *J. Am. Chem. Soc.*, 2008, **130**, 13850–13851.
27 S. Rapti, D. Sarma, S. A. Diamantis, E. Skliri, G. S. Armatas, A. C. Tsipis, Y. S. Hassan, M. Alkordi, C. D. Malliakas and M. G. Kanatzidis, *J. Mater. Chem. A*, 2017, **5**, 14707–14719.
28 A. D. Pournara, S. Rizogianni, D. A. Evangelou, E. K. Andreou, G. S. Armatas and M. J. Manos, *Chem. Commun.*, 2022, **58**, 8862–8865.
29 S. Ghosh, A. Rana, A. Patel, D. Manna and S. Biswas, *Environ. Sci.: Nano*, 2024, **11**, 1233–1244.
30 A. K. Rappé, C. J. Casewit, K. Colwell, W. A. Goddard III and W. M. Skiff, *J. Am. Chem. Soc.*, 1992, **114**, 10024–10035.
31 J. A. Timney, *Inorg. Chem.*, 1979, **18**, 2502–2506.
32 S. S. Hossain, V. Karthik, A. Dhakshinamoorthy and S. Biswas, *Inorg. Chem. Front.*, 2024, **11**, 142–155.
33 Y. Zhao, H. Zeng, X.-W. Zhu, W. Lu and D. Li, *Chem. Soc. Rev.*, 2021, **50**, 4484–4513.
34 S. Mostakim, M. R. U. Z. Khan, A. Das, S. Nandi, V. Trivedi and S. Biswas, *Dalton Trans.*, 2019, **48**, 12615–12621.
35 S. Ghosh, J. Krishnan, S. S. Hossain, A. Dhakshinamoorthy and S. Biswas, *ACS Appl. Mater. Interfaces*, 2023, **15**, 26843–26851.